RSC Advances

ROYAL SOCIETY OF CHEMISTRY

www.rsc.org/advances

Enhanced visible-light photocatalytic activity of $Ag_2O/g\text{-}C_3N_4$ p-n heterojunctions synthesized via photochemical route for degradation of tetracycline hydrochloride

Shuaishuai Ma,‡ Jinjuan Xue,‡ Yuming Zhou,* Zewu Zhang

School of Chemistry and Chemical Engineering, Southeast University, Nanjing 211189, P. R. China

Abstract The $Ag_2O/g\text{-}C_3N_4$ p-n heterojunctions were successfully fabricated by a facile photochemical method and applied as a photocatalyst in degradation of antibiotic tetracycline hydrochloride (TC-HCl) under visible light irradiation. The samples were well characterized by X-ray diffraction (XRD), energy-dispersive X-ray spectroscopy (EDS), transmission electron microscopy (TEM), and ultraviolet-visible diffuse reflectance spectroscopy (UV-vis DRS). The results demonstrated Ag_2O nanoparticles sized 5-15 nm were distributed on the surface of $g\text{-}C_3N_4$ to form the $Ag_2O/g\text{-}C_3N_4$ p-n heterojunctions. The heterojunctions were conducive to the high dispersibility of small Ag_2O nanoparticles and the efficient separation of photogenerated electron-hole pairs, resulting in the enhancement of photocatalytic activity by using $Ag_2O/g\text{-}C_3N_4$ heterojunctions as the photocatalyst compared to pure Ag_2O and $g\text{-}C_3N_4$ in TC-HCl degradation. In particular, the degradation rate of TC-HCl with was 1.21 and 3.52 times higher than that of pure Ag_2O and $g\text{-}C_3N_4$, respectively. Furthermore, the stability of the $Ag_2O/g\text{-}C_3N_4$ photocatalyst toward the degradation process under visible light irradiation was investigated.

* Corresponding author. Tel.: +86 25 52090617; fax: +86 25 52090617.
E-mail address: ymzhou@seu.edu.cn (Yuming Zhou).
‡S.S. Ma and J.J. Xue contributed equally to this work.

Introduction

Recently, antibiotic residues were found in the tap water in Nanjing city. Antibiotic residues could be discharged into the aquatic environment through various sources such as pharmaceutical industry, hospital effluent and excretion from human and livestock.[1] Tetracycline (TC) represents a major proportion of the antibiotics currently in use and tetracyclines were the most widely used antibacterial compounds in the United Kingdom according to Sarmah et al.'s report.[2] A report of the French Agency for Food Safety revealed that tetracycline represented more than half of the 1348.87 tons of antibiotics sold in 2007 in France.[3] Antibiotic TC residues in aqueous system have the potential to induce negative environmental effects even in low concentrations, including antibiotic resistance to bacteria, perturbations in ecosystems and possible risks to human health through drinking water and/or food-chain.[1, 4-6] As a result, water purifying from antibiotic residues is a highly essential issue for modern society. Semiconductor mediated photocatalysis has been the focus of recent research on antibiotic residues treatment, such as photocatalytic degradation of trimethoprim by metallic nanoparticles supported on TiO_2-P25,[7] TiO_2/5A composite catalyst for photocatalytic degradation of antibiotic oxytetracycline in aqueous solution,[8] and so on.

The polymeric semiconductor graphitic carbon nitride (g-C_3N_4) has recently attracted tremendous attention in photocatalysis area due to its advantages such as physical and chemical stability, response to visible-light, low cost, environmental friendliness and easy of availability.[9-13] Nevertheless, pure g-C_3N_4 suffers from shortcomings such as rapid recombination of photogenerated electron-hole pairs and low visible light utilization efficiency.[14, 15] Therefore, several approaches have been employed to modify g-C_3N_4-based photocatalysts with improved physicochemical properties and high photocatalytic activities.

For instance, construction of mesoporous structures,[16] doping with metal or non-metal species,[17-20] sensitizing with organic dyes,[21] formation of heterostructures by combining g-C_3N_4 with other semiconductors,[22-24] and so forth.

Ag_2O is a p-type semiconductor with a narrow energy band gap of 1.3 eV,[25] indicating that Ag_2O can respond to visible light very well. On account of that the combination of g-C_3N_4 and Ag_2O possess well matched overlapping band structure,[26] p-n heterojunctions could be fabricated by coupling Ag_2O with g-C_3N_4, which will bring more effective interface transfer of photogenerated electrons and holes to restrain the recombination. Besides, owe to its narrower band gap relative to g-C_3N_4 (2.7 eV), Ag_2O is able to act as efficient photosensitizer to enlarge the light response range under solar light irradiation and enhance the visible light photocatalytic performance of g-C_3N_4.[27-29]

In this paper, we applied a one-step photochemical process to successfully fabricate Ag_2O/g-C_3N_4 p-n heterojunctions. This method is simple and cost-effective without any expensive equipment, complex process control, and stringent reaction conditions. The as-prepared Ag_2O/g-C_3N_4 heterojunctions demonstrated to be a excellent photocatalyst which possess light adsorption ability in the whole UV-vis range and exhibited enhanced photocatalytic activity in degradation of antibiotic TC-HCl compared to that of pure Ag_2O and g-C_3N_4. Furthermore, the stability of the Ag_2O/g-C_3N_4 photocatalyst was investigated and a photocatalytic mechanism under visible-light irradiation was proposed.

Experimental section

Materials

Silver nitrate ($AgNO_3$), melamine and tetracycline hydrochloride (TC-HCl) were purchased from Aladdin Chemical Regent Co., Ltd. (Shanghai, China). All the reagents in this experiment are analytically pure and used without further purification.

Preparation of $Ag_2O/g\text{-}C_3N_4$ heterojunctions

$g\text{-}C_3N_4$ was synthesized by directly heating melamine in air atmosphere. Typically, 5 g of melamine was placed into quartz boats and heat-treated in a tube furnace at 550 ^oC for 4 h with a heating rate of 2 ^oC/min. Finally, the tube furnace was cooled to room temperature. The yellow products were collected and ground into powder for further use.

The typical preparation procedure of $Ag_2O/g\text{-}C_3N_4$ heterojunction photocatalyst was as follows and illustrated in Scheme 1 which is similar to our previous work[30]: 0.3 g of the as-prepared $g\text{-}C_3N_4$ power was dispersed in 100 mL deionized water with ultrasonication. Then, calculated amount of $AgNO_3$ dissolved in 20 mL deionized water was dropped into the above suspension. The mixture was stirred for 1 h in the absence of light to reach complete adsorption for Ag^+ ions on the surface of $g\text{-}C_3N_4$, then irradiated with a 250W high-pressure mercury lamp (λ = 365 nm) for 15 min with stirring. The resulting product was obtained by centrifugation, then washed with deionized water for several times and finally dried at 60 ^oC in vacuum overnight. By varying the amounts of $AgNO_3$ and $g\text{-}C_3N_4$, a series of $Ag_2O/g\text{-}C_3N_4$ composites with different mass ratios of 1:2, 1:1, 2:1, 3:1, 4:1 were all synthesized according to the above typical run. Pure Ag_2O sample was synthesized by a chemical precipitation method from $AgNO_3$ and NaOH aqueous solution.[31]

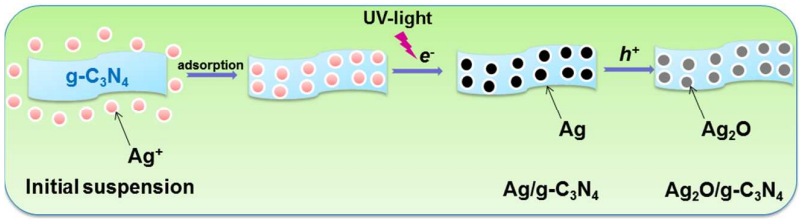

Scheme 1 Schematic illustration of the fabrication route of $Ag_2O/g\text{-}C_3N_4$ heterojunctions.

Sample characterizations

X-ray diffraction (XRD) measurement was carried out using a SmartLab XRD spectrometer (Rigaku) with Cu Kα radiation in the range of 10-80° (2θ). Energy dispersive X-ray spectroscopy (EDS) was used to analyze the composition of samples. Transmission electron microscopy (TEM; JEM-1230) and high resolution TEM (HRTEM) were used to characterize the morphologies of the products. UV-vis diffuse reflectance spectra (DRS) of the samples were recorded on a UV-vis spectrophotometer (UV-3600, Shimadzu) with an integrating sphere attachment. PL spectra were measured using room temperature photoluminescence with a 325 nm He-Cd laser excitation wavelength (Shimadzu RF-5301).

Photocatalytic activity test

The photocatalytic performance of the as-prepared samples were evaluated by degradation of antibiotic TC-HCl. 100 mg $Ag_2O/g\text{-}C_3N_4$ photocatalyst was added into 100 mL of 20 mg/L TC-HCl aqueous solution. A 500 W xenon lamp with a UV cut-off filter with $\lambda >$ 400 nm was used as the visible light source. Before irradiation, the suspension was stirred for 30 min in the dark for adsorption/desorption equilibrium between the photocatalyst and TC-HCl. Subsequently, the above suspension was irradiated in a photochemical chamber under continuously stirring with reflux water to keep its temperature constant. At certain time intervals, 3 mL solution was drawn out each time and centrifuged to get clear liquid. The

quantitative determination of TC-HCl was performed by measuring its intensity of the absorption peak with a UV-vis spectrophotometer. Comparative experiments of degradation TC-HCl by pure g-C_3N_4 and Ag_2O samples were also carried out.

Results and discussion

Structure and Morphology

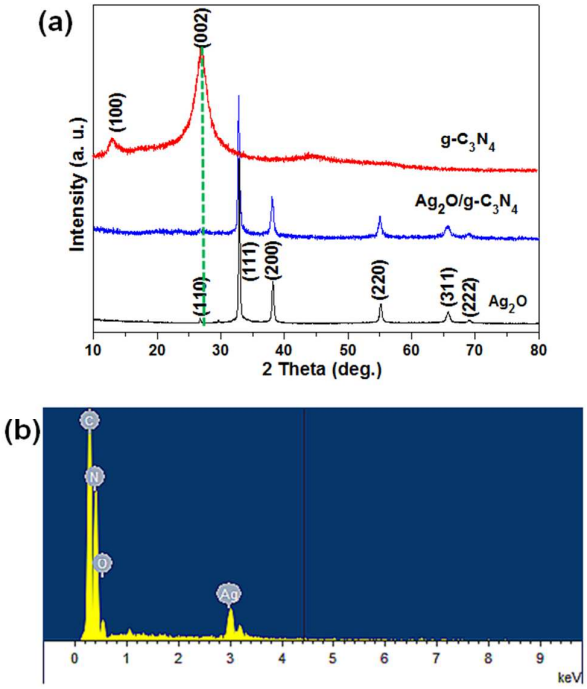

Fig. 1 XRD patterns of (a) g-C_3N_4, Ag_2O and Ag_2O/g-C_3N_4 heterojunctions (2:1), and EDS spectrum of (b) the Ag_2O/g-C_3N_4 (2:1).

Here, Ag_2O/g-C_3N_4 (2:1) was chosen as representative of Ag_2O/g-C_3N_4 heterojunctions on account of its good photocatalytic performance of TC-HCl photodegradation and appropriate amount of novel metal included in the photocatalyst (details given in later section). Fig. 1(a) shows the XRD patterns of the as-prepared g-C_3N_4, Ag_2O and Ag_2O/g-C_3N_4 heterojunctions. In pure g-C_3N_4 sample, there appeared two diffraction peaks at 2θ=13.1 ^{o} and

27.2° indexed to the (100) and (002) planes of hexagonal g-C_3N_4, which are arising from the characteristic inter-layer structural packing and the inter-planar stacking peaks of the aromatic systems, respectively.[32, 33] In pure Ag_2O sample, the diffraction peaks at 2θ = 26.8°, 32.8°, 38.1°, 54.9°, 65.4° and 68.7° correspond to the (110), (111), (200), (220), (311), and (222) planes of well-crystallized cubic Ag_2O (JCPDS 41-1104), respectively.[26, 28] For the Ag_2O/g-C_3N_4 sample, all the diffraction peaks can be indexed to the hexagonal phase g-C_3N_4 and the cubic phase Ag_2O. No characteristic peaks for other impurities were observed, indicative of the high purity of the product. In addition, the weak peak of Ag_2O at 26.8° cannot be observed in the XRD pattern of the Ag_2O/g-C_3N_4 sample due to it may be covered by the broad peak of g-C_3N_4 at 27.2°. EDS analysis was employed to investigate the composition of the heterojunctions (in Fig. 1(b)), where the appeared peaks confirm that the product was only composed of C, N, O and Ag elements.

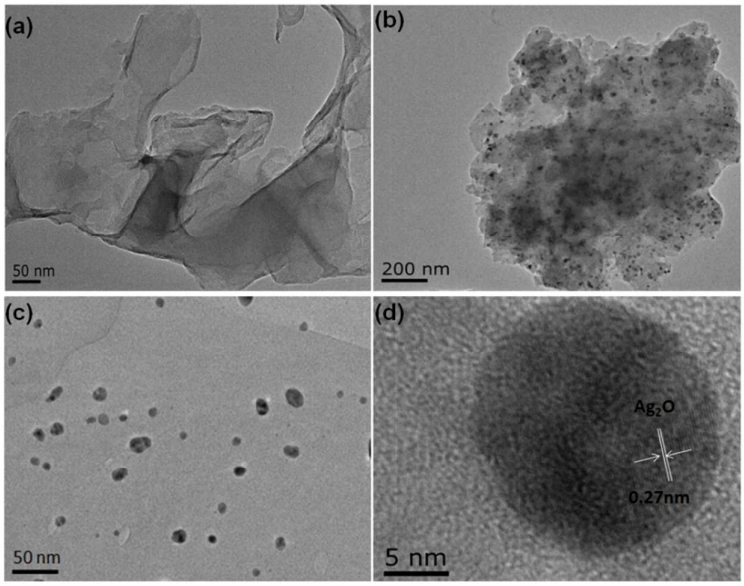

Fig.2 Typical TEM images of (a) g-C_3N_4, (b, c) Ag_2O/g-C_3N_4 (2:1) and HRTEM (d) image of the as-prepared Ag_2O/g-C_3N_4 heterojunctions (2:1).

The morphologies of pure g-C_3N_4 and Ag_2O/g-C_3N_4 heterojunctions (2:1) were

investigated by transmission electron microscopy (TEM) and high resolution TEM (HRTEM), as shown in Fig. 2. Fig. 2(a) shows that g-C_3N_4 has a layer structure and is a thin sheet with irregular morphology. For the Ag_2O/g-C_3N_4 sample in Fig. 2(b and c), it can be observed that Ag_2O nanoparticles sized of 5-15 nm are closely and uniformly anchored on the surface of g-C_3N_4 to form the heterojunctions. By measuring the lattice fringes in HRTEM image (Fig. 2(d)), the resolved interplanar distance of 0.27 nm agrees well with the lattice spacing of the (111) plane of Ag_2O. According to our previous report, pure Ag_2O nanoparticles prepared by the precipitation method possess an irregular spherical morphology with an average diameter of approximately 100 nm.[34] Apparently, Ag_2O nanoparticles in Ag_2O/g-C_3N_4 heterojunctions system synthesized by the photochemical method are smaller with diameters than that of pure Ag_2O. It could be resulted from that g-C_3N_4 acts as the support for the particles to prevent the agglomeration, leading to the small size and high dispersibility of Ag_2O nanoparticles. Such special morphology and structure of the as-prepared Ag_2O/g-C_3N_4 heterojunctions should be propitious to effective separation of the photogenerated charge carriers and thus enhance the photocatalytic efficiency.[35]

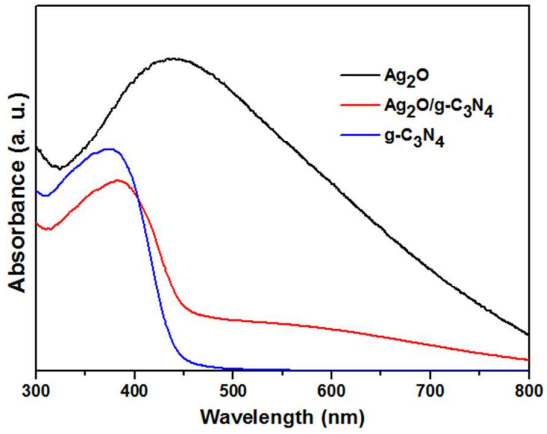

Fig. 3 UV-Vis diffuse reflectance spectra of g-C_3N_4, Ag_2O and Ag_2O/g-C_3N_4 heterojunctions (2:1).

The optical absorption plays an important role in the photocatalysis, especially in the

visible-light photodegradation of contaminants. The optical absorption properties of g-C_3N_4, Ag_2O and Ag_2O/g-C_3N_4 heterojunctions (2:1) were measured by UV-Vis DRS and demonstrated in Fig. 3. For pure g-C_3N_4, an adsorption edge can be observed at 460 nm and the absorption band is lower than 460 nm. After introducing Ag_2O, the Ag_2O/g-C_3N_4 heterojunctions exhibit light absorption in the whole UV-vis range. It can be seen that pure Ag_2O exhibits a wide and strong light absorption in the whole UV-vis range of 200-800 nm. Therefore, the significant improvement on visible-light response of the heterojunctions is assigned to the excellent visible light absorption property of Ag_2O. Benefiting from this enlarged light absorption range, the Ag_2O/g-C_3N_4 heterojunctions are expected to achieve more efficient utilization of the solar light than that of pure g-C_3N_4 and show enhanced photocatalytic activity.

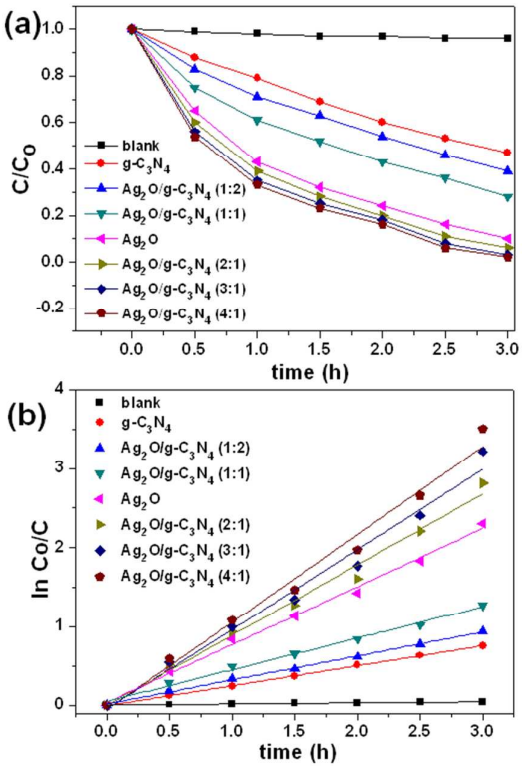

Fig. 4 Photocatalytic activities (a) and kinetics (b) of the as-prepared g-C_3N_4, Ag_2O and Ag_2O/g-C_3N_4

heterojunctions with different mass ratios for degradation of TC-HCl under visible light irradiation.

Photocatalytic Activity

Fig. 4 presents the corresponding concentration change of TC-HCl and the reaction rate (k) as the function of visible light irradiation time for g-C_3N_4, Ag_2O and Ag_2O/g-C_3N_4 samples as the different photocatalysts. Where, C_o and C are the equilibrium concentrations of TC-HCl before and after visible light irradiation, respectively. As can be seen in Fig. 4(a), when using pure g-C_3N_4 as the photocatalysts, inefficient visible light photocatalytic activity is observed and the degradation rate of TC-HCl is only about 52.8% after visible light irradiated for 3 h. Whereas pure Ag_2O shows a good visible-light photocatalytic activity and the degradation rate of TC-HCl reaches 89% in 3 h. In the case of the different Ag_2O/g-C_3N_4 samples, the sample based on the 2:1 ratio exhibits better photocatalytic activity than the samples with 1:2 and 1:1 ratios, where the degradation rate of TC-HCl can reach 94% under the same irradiation time. With increasing the amount of Ag_2O in the composites, the Ag_2O/g-C_3N_4 (3:1, 4:1) shows a little improvement rather than particularly great progress in photocatalytic efficiency. As we know, the consumption of a large amount of the noble metal of silver strongly limits novel mental based photocatalyst practical environmental applications. Therefore, to achieve the improvement in photocatalytic activity only by increasing the amount of Ag_2O does not meet the practical application. We take 2:1 (Ag_2O:g-C_3N_4) as a proper ratio with respect to both of the photocatalytic activity and the consumption amount of the noble metal of silver, then selected Ag_2O/g-C_3N_4 heterojunctions (2:1) for further research. Moreover, the reaction rates of the g-C_3N_4, Ag_2O and Ag_2O/g-C_3N_4 heterojunctions (2:1) calculated from Fig. 4(b) are 0.2539, 0.7353, 0.8929 min^{-1}, respectively. Obviously, the photodegradation rate of the Ag_2O/g-C_3N_4

heterojunctions (2:1) is around 1.21 times faster than that of the Ag_2O, and over 3.5 times faster than that of pure g-C_3N_4, indicating the Ag_2O/g-C_3N_4 heterojunctions (2:1) are much prominent visible light photocatalyst for degradation of antibiotic TC-HCl.

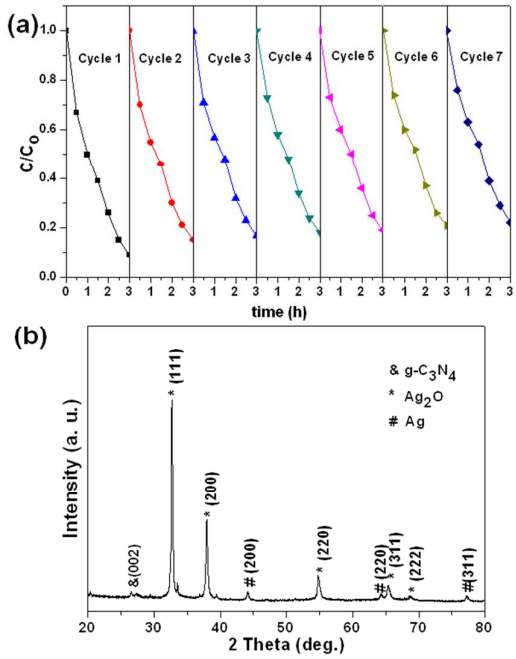

Fig. 5 (a) Seven photocatalytic degradation cycles of TC-HCl using Ag_2O/g-C_3N_4 heterojunctions (2:1) under visible light irradiation, and (b) the XRD pattern of the as-prepared Ag_2O/g-C_3N_4 heterojunctions after the repeated photocatalytic degradation experiments for seven times under visible light irradiation.

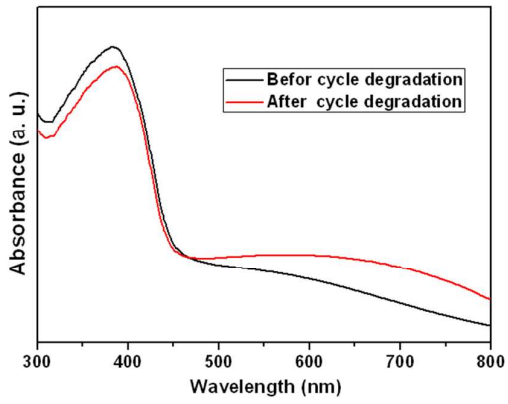

Fig. 6 UV-Vis diffuse reflectance spectra of the sample before and after cycle degradation.

The stability is very important for recycling of the catalyst based on its importance for

practical application. The cycling test of the visible light driven photocatalysis of the Ag_2O/g-C_3N_4 heterojunctions (2:1) in decokmposing TC-HCl is shown in Fig. 5(a). Only a slight decrease of the photocatalytic enficency after seven photocatalysis cycles is observed, meaning the Ag_2O/g-C_3N_4 heterojunctions have good stability and reusability. Furthermore, the Ag_2O/g-C_3N_4 heterojunction photocatalyst after seven cycling test was collected and characterized by XRD. It is noted that three new diffraction peaks appeared in the XRD pattern, which can be indexed to (200), (220) and (311) plans of metallic Ag^0 (JCPDS 04-0783). The presence of Ag^0 indicates that Ag_2O was partially transformed to Ag^0 via in situ photoreduction during the photocatalysis process. Previous research results demonstrated that, after the formation of a certain amount of metallic Ag, the obtained Ag_2O/Ag exhibits a stable structure.[36] And the novel mental Ag also can act as the electron-sink to restrain the recombination of charge carriers by a fast transfer of photogenerated electrons onto Ag, giving an improvement on the photocatalytic activity of the catalyst.[37] In addition, Fig. 6 shows the UV-Vis diffuse reflectance spectra of the sample before and after cycle degradation. Notably, the absorbance intensity in the range of 450-800 nm was increased after cycle degradation, which could be attributed to the characteristic absorption of the SPR of Ag nanoparticles.[38] This also suggests the presence of metallic Ag nanoparticles in the cycled sample, consistent with the XRD result in Fig. 5(b).

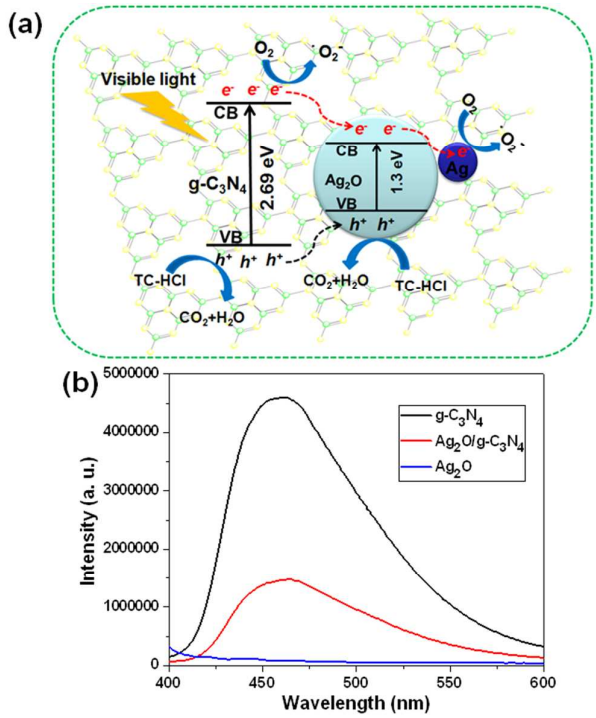

Fig. 7 (a) Proposed mechanisms for the photocatalysis of the Ag_2O/g-C_3N_4 heterojunctions under visible light irradiation, (b) PL emission spectra of Ag_2O, g-C_3N_4 and Ag_2O/g-C_3N_4 heterojunctions.

Photocatalytic Mechanism

On the basis of the above results, a possible photocatalytic mechanism of the Ag_2O/g-C_3N_4 heterojunction photocatalyst under visible light irradiation was proposed and illustrated in Fig. 7(a). Under visible light irradiation, both g-C_3N_4 and Ag_2O are simultaneously excited to produced h^+ and e^-. Due to the inner electric field existed in p-n heterojunctions, the photogenerated electrons will have a tendency to transfer from Ag_2O to g-C_3N_4 in Ag_2O/g-C_3N_4 composites, while the holes have an opposite transfer.[26, 29] However, the CB of g-C_3N_4 (-1.12 V, vs SHE) lays above that of Ag_2O (0.20 V, vs SHE),[36, 39] so the photogenerated electrons in g-C_3N_4 would inject into the CB of Ag_2O. As a result, the transfer of electrons between g-C_3N_4 and Ag_2O is restricted to some extent, while the transfer of holes can be accelerated, resulting in an efficient separation of photogenerated charge carriers and thus enhanced the photocatalytic

activity. As confirmed by above XRD analysis, Ag_2O was partially in situ reduced to Ag^0 during the photocatalysis process, and Ag also can act as the electron-sink to restrain the recombination of charge carriers by a fast transfer of photogenerated electrons , which would be trapped by O_2 to produce$\bullet O_2$. The photogenerated electrons left on the CB of g-C_3N_4 also can react with O_2 to produce active species $\bullet O_2^-$. Besides, the E_{VB} (g-C_3N_4, +1.57 eV vs SHE; Ag_2O, +1.4 eV vs SHE) values were lower than the standard redox potential of $\bullet OH/H_2O$ (+2.68 eV vs SHE),[28, 40] indicating that the photogenerated holes on g-C_3N_4 and Ag_2O could not oxidize H_2O to active species •OH. Therefore, h^+ on the VB of g-C_3N_4 and Ag_2O would react with TC-HCl directly. Furthermore, the better separation efficiency of photogenerated electrons and holes in Ag_2O/g-C_3N_4 p-n heterojunctions compared to pure g-C_3N_4 was confirmed by Photoluminescence (PL) spectra. PL emission intensity is related to the recombination rate of excited electron-hole pairs. Lower intensity indicates more excited electrons are transferred or trapped, and higher intensity means the faster the recombination rate.[41] It was generally believed that a higher PL intensity always indicated a faster recombination of photogenerated electrons and holes. Fig. 7(b) shows the PL spectra of pure g-C_3N_4, Ag_2O, and Ag_2O/g-C_3N_4 composites at an excitation wavelength of 325 nm. As can be observed, the wide emission peak of pure g-C_3N_4 was at about 460 nm, which was ascribed to the band-gap recombination of electron-hole pairs. The presence of Ag_2O could not change the emission peak position but rather reduced its relative intensity compared with pure g-C_3N_4. This indicated that the recombination of the photogenerated charge carrier was inhibited greatly in the Ag_2O/g-C_3N_4 p-n heterojunctions. Thus, the lifetime of the excited electrons and holes can be prolonged in the transfer process, inducing higher quantum efficiency, causing the enhanced photocatalytic

activity of the as-prepared Ag_2O/g-C_3N_4 p-n heterojunctions.

Conclusions

In summary, we have successfully fabricated Ag_2O/g-C_3N_4 p-n heterojunctions by depositing small Ag_2O nanoparticles sized of 5-15 nm on the surface of g-C_3N_4 via a facile photochemical route. The obtained Ag_2O/g-C_3N_4 p-n heterojunctions exhibited enhanced photocatalytic activity toward antibiotic TC-HCl degradation under visible light irradiation than that of pure g-C_3N_4 and Ag_2O nanoparticles. Such enhanced photocatalytic activity of the Ag_2O/g-C_3N_4 p-n heterojunctions could be attributed to high dispersibility of small Ag_2O nanoparticles, improved optical absorption property as well as the effective separation of the photogenerated electrons and holes. Thus, the Ag_2O/g-C_3N_4 p-n heterojunctions can be a promising candidate for efficient visible light driven photocatalytic systems for antibiotic residues removal.

Acknowledgements

The authors are grateful to the financial supports of National Natural Science Foundation of China (Grant No. 21376051, 21306023, 21106017, and 51077013), Natural Science Foundation of Jiangsu (Grant No. BK20131288), Fund Project for Transformation of Scientific and Technological Achievements of Jiangsu Province of China (Grant No. BA2014100) and the Fundamental Research Funds for the Central Universities (KYLX_0161).

References

1. A. G. Trovo, R. F. P. Nogueira, A. Aguera, A. R. Fernandez-Alba and S. Malato, *Water. Res.*, 2011, **45**, 1394-1402.

2. A. K. Sarmah, M. T. Meyer and A. B. A. Boxall, *Chemosphere*, 2006, **65**, 725-759.

3. A. Chevance, G. Moulin, F. AFSSA-ANMV and P. AFSSA, *Fougères, 38pp*, 2009.

4. T. P. H. Phan, S. Managaki, N. Nakada, H. Takada, A. Shimizu, D. H. Anh, P. H. Viet and S. Suzuki, *Sci. Total. Environ.*, 2011, **409**, 2894-2901.

5. V. Homem, A. Alves and L. Santos, *Sci. Total. Environ.*, 2010, **408**, 6272-6280.

6. Y. J. Lee, S. E. Lee, D. S. Lee and Y. H. Kim, *Environ. Toxicol. Phar.*, 2008, **26**, 216-221.

7. S. Oros-Ruiz, R. Zanella and B. Prado, *J. Hazard. Mater.*, 2013, **263**, 28-35.

8. C. Zhao, Y. Zhou, D. J. de Ridder, J. Zhai, Y. M. Wei and H. P. Deng, *Chem. Eng. J.*, 2014, **248**, 280-289.

9. X. D. Zhang, X. Xie, H. Wang, J. J. Zhang, B. C. Pan and Y. Xie, *J. Am. Chem. Soc.*, 2013, **135**, 18-21.

10. S. B. Yang, Y. J. Gong, J. S. Zhang, L. Zhan, L. L. Ma, Z. Y. Fang, R. Vajtai, X. C. Wang and P. M. Ajayan, *Adv. Mater.*, 2013, **25**, 2452-2456.

11. J. Mao, T. Y. Peng, X. H. Zhang, K. Li, L. Q. Ye and L. Zan, *Catal. Sci. Technol.*, 2013, **3**, 1253-1260.

12. A. B. Jorge, D. J. Martin, M. T. S. Dhanoa, A. S. Rahman, N. Makwana, J. W. Tang, A. Sella, F. Cora, S. Firth, J. A. Darr and P. F. McMillan, *J. Phys. Chem. C*, 2013, **117**, 7178-7185.

13. G. H. Dong and L. Z. Zhang, *J. Mater. Chem.*, 2012, **22**, 1160-1166.

14. J. H. Liu, Y. W. Zhang, L. H. Lu, G. Wu and W. Chen, *Chem. Commun.*, 2012, **48**, 8826-8828.

15. B. Chai, T. Y. Peng, J. Mao, K. Li and L. Zan, *Phys. Chem. Chem. Phys.*, 2012, **14**, 16745-16752.

16. F. Z. Su, S. C. Mathew, G. Lipner, X. Z. Fu, M. Antonietti, S. Blechert and X. C. Wang, *J. Am.*

Chem. Soc., 2010, **132**, 16299-16301.

17. X. F. Chen, J. S. Zhang, X. Z. Fu, M. Antonietti and X. C. Wang, *J. Am. Chem. Soc.*, 2009, **131**, 11658-11659.

18. Y. Di, X. C. Wang, A. Thomas and M. Antonietti, *Chemcatchem*, 2010, **2**, 834-838.

19. G. Liu, P. Niu, C. H. Sun, S. C. Smith, Z. G. Chen, G. Q. Lu and H. M. Cheng, *J. Am. Chem. Soc.*, 2010, **132**, 11642-11648.

20. Y. J. Zhang, T. Mori, J. H. Ye and M. Antonietti, *J. Am. Chem. Soc.*, 2010, **132**, 6294-6295.

21. H. J. Yan and Y. Huang, *Chem. Commun.*, 2011, **47**, 4168-4170.

22. J. Fu, B. B. Chang, Y. L. Tian, F. N. Xi and X. P. Dong, *J. Mater. Chem. A*, 2013, **1**, 3083-3090.

23. X. S. Zhou, B. Jin, L. D. Li, F. Peng, H. J. Wang, H. Yu and Y. P. Fang, *J. Mater. Chem.*, 2012, **22**, 17900-17905.

24. W. Liu, M. L. Wang, C. X. Xu and S. F. Chen, *Chem. Eng. J.*, 2012, **209**, 386-393.

25. L. H. Tjeng, M. B. J. Meinders, J. Vanelp, J. Ghijsen, G. A. Sawatzky and R. L. Johnson, *Phys. Rev. B*, 1990, **41**, 3190-3199.

26. M. Xu, L. Han and S. J. Dong, *Acs Appl. Mater. Inter.*, 2013, **5**, 12533-12540.

27. H. T. Ren, S. Y. Jia, S. H. Wu, T. H. Zhang and X. Han, *Mater. Lett.*, 2015, **142**, 15-18.

28. L. Shi, L. Liang, J. Ma, F. X. Wang and J. M. Sun, *Catal. Sci. Technol.*, 2014, **4**, 758-765.

29. H. T. Ren, S. Y. Jia, Y. Wu, S. H. Wu, T. H. Zhang and X. Han, *Ind. Eng. Chem. Res.*, 2014, **53**, 17645-17653.

30. S. S. Ma, J. J. Xue, Y. M. Zhou and Z. W. Zhang, *J. Mater. Chem. A*, 2014, **2**, 7272-7280.

31. W. J. Zhou, H. Liu, J. Y. Wang, D. Liu, G. J. Du and J. J. Cui, *Acs Appl. Mater. Inter.*, 2010, **2**,

2385-2392.

32. J. H. Liu, T. K. Zhang, Z. C. Wang, G. Dawson and W. Chen, *J. Mater. Chem.*, 2011, **21**, 14398-14401.

33. J. X. Sun, Y. P. Yuan, L. G. Qiu, X. Jiang, A. J. Xie, Y. H. Shen and J. F. Zhu, *Dalton T.*, 2012, **41**, 6756-6763.

34. J. J. Xue, S. S. Ma, Y. M. Zhou, Z. W. Zhang, X. Wu and C. G. She, *Rsc Adv.*, 2015, **5**, 3122-3129.

35. L. Y. Huang, H. Xu, Y. P. Li, H. M. Li, X. N. Cheng, J. X. Xia, Y. G. Xu and G. B. Cai, *Dalton T.*, 2013, **42**, 8606-8616.

36. X. F. Wang, S. F. Li, H. G. Yu, J. G. Yu and S. W. Liu, *Chem. Eur. J.*, 2011, **17**, 7777-7780.

37. W. Y. Gao, M. Q. Wang, C. X. Ran, X. Yao, H. H. Yang, J. Liu, D. L. He and J. B. Bai, *Nanoscale*, 2014, **6**, 5498-5508.

38. P. Hu, X. L. Hu, C. J. Chen, D. F. Hou and Y. H. Huang, *Crystengcomm*, 2014, **16**, 649-653.

39. S. C. Yan, S. B. Lv, Z. S. Li and Z. G. Zou, *Dalton T.*, 2010, **39**, 1488-1491.

40. S. Kumar, T. Surendar, A. Baruah and V. Shanker, *J. Mater. Chem. A*, 2013, **1**, 5333-5340.

41. L. C. Sim, K. H. Leong, S. Ibrahim and P. Saravanan, *J. Mater. Chem. A*, 2014, **2**, 5315-5322.